ELSEVIER

Journal of Fluids and Structures 22 (2006) 295–314

JOURNAL OF FLUIDS AND STRUCTURES

www.elsevier.com/locate/jfs

Interaction of railway vehicles with track in cross-winds

Y.L. Xu[a,*], Q.S. Ding[a,b]

[a]*Department of Civil and Structural Engineering, The Hong Kong Polytechnic University, Kowloon, Hong Kong, China*
[b]*Department of Bridge Engineering, Tongji University, Shanghai 200092, China*

Received 14 February 2005; accepted 19 November 2005
Available online 24 January 2006

Abstract

This paper presents a framework for simulating railway vehicle and track interaction in cross-wind. Each 4-axle vehicle in a train is modeled by a 27-degree-of-freedom dynamic system. Two parallel rails of a track are modeled as two continuous beams supported by a discrete-elastic foundation of three layers with sleepers and ballasts included. The vehicle subsystem and the track subsystem are coupled through contacts between wheels and rails based on contact theory. Vertical and lateral rail irregularities simulated using an inverse Fourier transform are also taken into consideration. The simulation of steady and unsteady aerodynamic forces on a moving railway vehicle in cross-wind is then discussed in the time domain. The Hilber–Hughes–Taylor α-method is employed to solve the nonlinear equations of motion of coupled vehicle and track systems in cross-wind. The proposed framework is finally applied to a railway vehicle running on a straight track substructure in cross-wind. The safety and comfort performance of the moving vehicle in cross-wind are discussed. The results demonstrate that the proposed framework and the associated computer program can be used to investigate interaction problems of railway vehicles with track in cross-wind.

Keywords: Railway vehicles; Vehicle–track interaction; Cross-wind; Simulation; Safety

1. Introduction

Dynamic response of railway vehicles running on a railway track has been a subject of great interest to vehicle designers, maintenance engineers, as well as track designers for many years. This interest is motivated by the desire to improve ride quality, to reduce wear to vehicle and track components, to prevent vehicle hunting and, most important of all, to ensure safe operation. With ever-increasing trailing tonnage and higher running speeds, it becomes more important to further improve the performance of railway vehicles and their suspension system.

Early studies (Jenkins et al., 1974; Newton and Clark, 1979; Grassie et al., 1982) on vibration of a railway track under moving vehicles did not take into consideration the coupling effects between vehicles and railway track. Later, several models were developed to consider the coupling of vehicles and railway track (Cai and Raymond, 1992; Dahlberg, 1995; Nielsen, 1993; Zhai and Sun, 1994). For instance, Cai and Raymond (1992) reported a track dynamic model with one bogie to examine the effect of various wheel and rail defects on dynamic responses. Zhai and Sun (1994) presented a more detailed coupled model in which the wagon with two bogies was represented by two multi-body systems and the

*Corresponding author. Tel.: +852 2766 6050; fax: +852 2334 6389.
E-mail address: ceylxu@polyu.edu.hk (Y.L. Xu).

0889-9746/$ - see front matter
doi:10.1016/j.jfluidstructs.2005.11.003

track was modeled as an infinite Euler beam supported on a discrete-elastic foundation consisting of three layers with sleeper and ballast included. Furthermore, the coupled vehicle–track model in the vertical direction was extended to include interactive vibration of vehicle and track in the lateral direction (Zhai et al., 1996; Diana et al., 1994). A review report on modelling vehicle and track interaction can be found in Knothe and Grassie (1993).

The aerodynamic forces on a railway vehicle moving through a cross-wind may be sufficiently large to overturn the vehicle. To be able to guarantee comfort and safety for a vehicle in cross-wind, one has to understand the effects of cross-winds on the dynamic interaction between the vehicle subsystem and the track subsystem. However, compared with studies on vehicle and track interaction, researches on the interaction of vehicles with track in cross-wind are relatively few. Balzer (1977) developed a theory to estimate aerodynamic forces on a moving vehicle, in which Taylor's hypothesis of "frozen turbulence" was employed. For engineering applications, Cooper (1984) proposed the power spectral density (PSD), square-root coherence function, phase-lag function and aerodynamic admittance function for unsteady side forces on a moving vehicle and laid down a foundation for investigating wind effects on a moving vehicle in the frequency domain. Baker (1991a,b) further investigated both steady and unsteady aerodynamic forces on a variety of vehicles and carried out extensive studies on the interaction between aerodynamic forces and moving vehicles.

This study focuses on the simulation of dynamic response of railway vehicles running on a track in cross-wind in the time domain. Each 4-axle vehicle in a train is modeled by a 27-degree-of-freedom dynamic system. Two parallel rails of a track are modeled as two continuous beams supported by a discrete-elastic foundation of three layers with sleepers and ballasts included. The vehicle subsystem and the track subsystem are coupled through contacts between wheels and rails based on the contact theory. Vertical and lateral rail irregularities simulated using an inverse Fourier transform are also taken into consideration. The steady and unsteady aerodynamic forces on a moving railway vehicle in cross-wind are derived and simulated in the time domain. The Hilber–Hughes–Taylor α-method is employed to solve the nonlinear equations of motion of coupled vehicle and track systems in cross-wind. The proposed framework is finally applied to a railway vehicle running on a straight track substructure in cross-wind. The safety and comfort performance of the moving vehicle in cross-wind are discussed.

2. Vehicle–track interaction model

In this study, the coupled vehicle and track system is first divided into two subsystems: the vehicle subsystem and the track subsystem. The dynamic model is then established for each subsystem. The two subsystems are finally coupled through contacts between wheels and rails based on contact theory, in which rail irregularities are included but suspension stops and wheel lift-off are not considered. Since the coupled vehicle and track system is considered in cross-wind, the motions of the coupled vehicle–track system in both the vertical and lateral directions are reflected in the modelling.

2.1. Modelling of vehicle subsystem

A 4-axle railway vehicle with two suspension systems, which is a common railway vehicle used in China, is taken as an example to demonstrate the modelling of vehicle subsystem (see Fig. 1). The vehicle consists of a car body, two bogies, four wheel-sets, and the connections between the three components. To simplify the analysis but with enough accuracy, the following assumptions are used in the modelling of the vehicle subsystem:

(i) the vehicle is running on a straight railway track at a constant velocity V_T;
(ii) the car body, bogies and wheel-sets are regarded as rigid components, neglecting their elastic deformation during vibration;
(iii) the connections between a bogie and a wheel-set are characterized by two linear springs and two viscous dashpots of the same properties in either the horizontal direction or the vertical direction, named the first suspension system;
(iv) the connections between the car body and a bogie are represented by two linear springs and two viscous dashpots of the same properties in either the horizontal direction or the vertical direction, named the secondary suspension system.

The car body or each bogie is assigned five degrees of freedom: the vertical displacement Y, the lateral displacement Z, the roll displacement θ, the yaw displacement φ, and the pitch displacement ϕ with respect to its mass center. Each wheel-set has three degrees of freedom: the vertical displacement Y_w, the lateral displacement Z_w, and the roll displacement θ_w with respect to its mass center. As a result, the total degrees of freedom of the vehicle are 27. The nodal

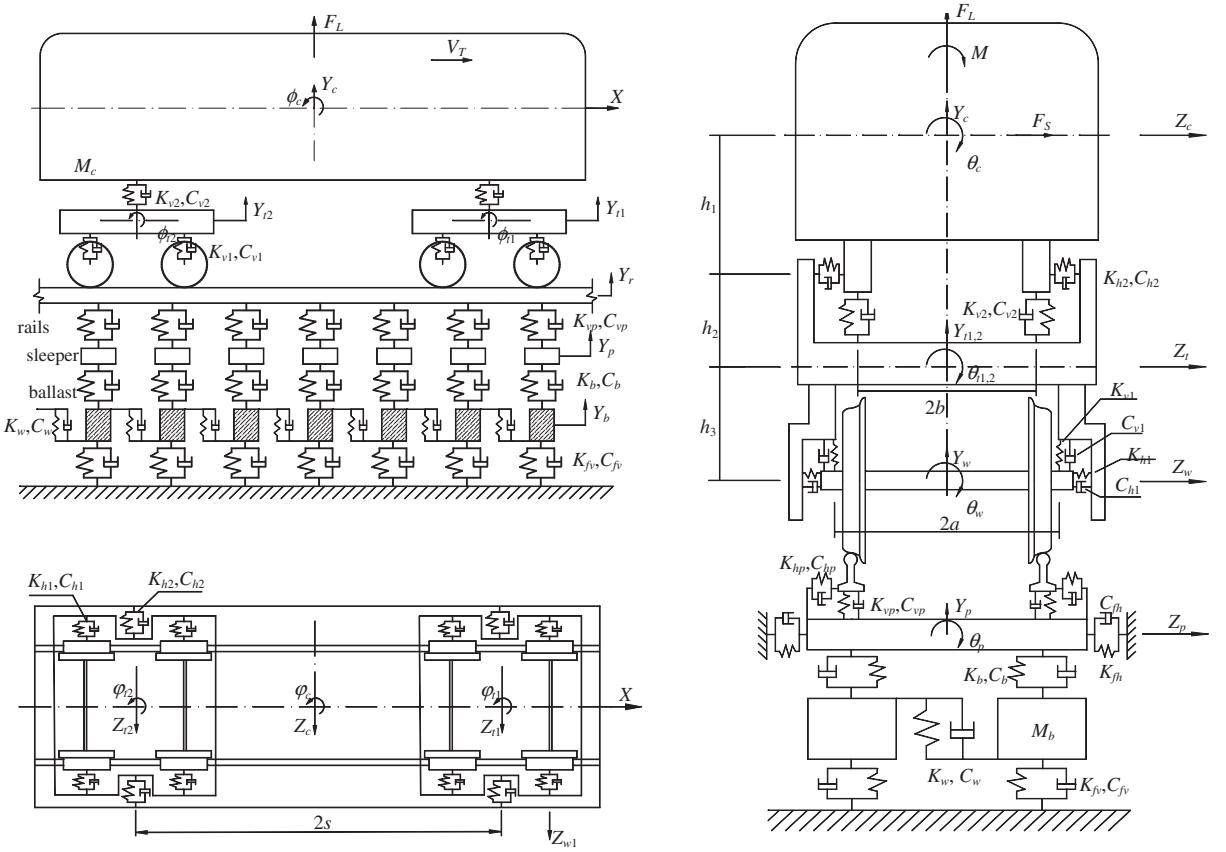

Fig. 1. Modelling of vehicle and track interaction in cross-wind.

displacement vector of the vehicle can be written as

$$X_v^{\mathrm{T}} = \{X_c^{\mathrm{T}}, X_{t1}^{\mathrm{T}}, X_{t2}^{\mathrm{T}}, X_{w1}^{\mathrm{T}}, X_{w2}^{\mathrm{T}}, X_{w3}^{\mathrm{T}}, X_{w4}^{\mathrm{T}}\}, \tag{1}$$

where X_v is the 27×1 displacement vector of the vehicle; X_c, X_t, X_w are the displacement vectors of the car body, bogies, and wheel-sets, respectively; the subscript 1 or 2 indicates the first bogie (or wheel-set) and the second bogie (or wheel-set), respectively; and the superscript T indicates the transpose operation. By assuming that displacement responses of vehicle components are small, the equation of motion of the vehicle subsystem with respect to the static equilibrium position can be derived using the Lagrangian approach as follows:

$$M_v\ddot{X}_v + C_v\dot{X}_v + K_vX_v = F_v^c + F_v^w, \tag{2}$$

where M_v, C_v, K_v are the 27×27 mass, stiffness and damping matrices of the vehicle subsystem, respectively; each dot in the vector X_v denotes the partial differentiation with respect to time t; F_v^c is the vector of forces exerted by the track subsystem on the vehicle subsystem with respect to the mass center of the wheel-set; and F_v^w is the vector of wind forces acting on the car body with respect to its mass center. The detailed derivation of Eq. (2) can be referred to the literature (Xu et al., 2004) while the two force vectors will be discussed in the subsequent sections.

2.2. Modelling of track subsystem

The track subsystem consists of rails, sleepers, and ballasts. The two parallel rails of the track are modeled as two continuous beams supported on a discrete-elastic foundation consisting of three layers with sleepers and ballasts included (see Fig. 1). In consideration that the frequency range of interest for the coupled vehicle–track system in cross-wind is below 30 Hz, sleepers and ballasts can be regarded as rigid bodies. The connections between the rails and the

sleepers are represented by linear springs and viscous dashpots of the same properties in either the horizontal direction or the vertical direction. The connections between the sleepers and the ballasts are represented by linear springs and viscous dashpots of the same properties in the vertical direction. The horizontal stiffness and damping of both the sleeper and the ballast are modeled by linear springs and viscous dashpots horizontally installed at the ends of the sleeper against the ground. In order to account for shearing continuity of the particles between the adjacent ballasts, linear spring and viscous dashpot are introduced between the adjacent ballasts to model shear coupling effects. Moreover, the ballasts are connected to the ground through linear springs and viscous dashpots in the vertical direction.

In the modelling, the rail between two adjacent sleepers is taken as one beam element. The degrees of freedom of the beam element in the longitudinal (x-) and torsional directions are not considered. Each sleeper has three degrees of freedom and each ballast block has one degree of freedom in the vertical direction only. As a result, the nodal displacement vector of the track subsystem at the ith sleeper can be written as

$$X_{si}^{\mathrm{T}} = \{Y_{rl}, Z_{rl}, \theta_{rl}^{Y}, \theta_{rl}^{Z}, Y_{rr}, Z_{rr}, \theta_{rr}^{Y}, \theta_{rr}^{Z}, Y_{p}, Z_{p}, \theta_{p}, Y_{bl}, Y_{br}\}, \tag{3}$$

where the first subscripts r, p, and b, stand for the rail, sleeper, and ballast, respectively; the second subscripts l and r stand for left and right side, respectively; and the superscripts Y and Z stand for the axis around which the beam rotates.

In terms of the general procedure of finite element method, the equation of motion of the track subsystem can be assembled as

$$M_s\ddot{X}_s + C_s\dot{X}_s + K_sX_s = F_s^c, \tag{4}$$

where M_s, C_s and K_s are the mass, stiffness and damping matrix of the track subsystem, respectively; X_s is the total nodal displacement vector of the track subsystem; and F_s^c is the vector of the contact forces transmitted from the wheels to the rails at all contact points, which will be discussed in the subsequent section.

2.3. Wheel and rail interaction

Wheel and rail interaction is an essential element that couples the vehicle subsystem with the track subsystem. The interaction between a wheel and a rail involves two basic issues: the geometric relationship and the contact forces between the wheel and the rail.

As mentioned before, each wheel-set has three degrees of freedom: the vertical, lateral, and rolling motions with respect to its mass center. In this study, the vertical motion of the wheel-set is assumed to be independent of its lateral and rolling motions. The rolling displacement of the wheel-set consists of two parts: one is due to nonuniform configurations of the right and left rails; and the other is the rolling angle induced by the lateral displacement of the wheel-set relative to the rails due to the profiles of the wheel and rail cross-sections. Before simulating the interaction of vehicle and track in cross-wind, a geometric analysis should be carried out to find the geometric contact information as a function of the lateral displacement of the wheel-set. The geometric contact information includes, but it is not limited to, the relative rolling angle of the wheel-set to the rails, the position of the contact point between the wheel and rail, the contact angle at contact point between the wheel and rail, and the radius of curvature at contact point for either wheel or rail. Under strong cross-wind, the lateral displacement of the wheel-set relative to the rails may be large, which may cause a strong nonlinearity in the geometric relationship.

Based on the Kalker creepage theory (Kalker, 1990), the creeping forces between the wheel and rail can be calculated as

$$T_x = -f_{11}\xi_x, \tag{5a}$$

$$T_z = -f_{22}\xi_z - f_{23}\xi_{sp}, \tag{5b}$$

$$M_{sp} = -f_{23}\xi_z - f_{33}\xi_{sp}, \tag{5c}$$

where T_x, T_z, and M_{sp} are the longitudinal creeping force, lateral creeping force, and spin creeping moment, respectively; f_{11}, f_{22}, f_{23}, and f_{33} are the creepage coefficients; ξ_x, ξ_z, and ξ_{sp} are the creepage ratios in the longitudinal, lateral, and spin directions respectively, and they can be expressed as follows:

$$\xi_x = \frac{V_{wx} - V_{rx}}{V_T}, \quad \xi_z = \frac{V_{wz} - V_{rz}}{V_T}, \quad \xi_{sp} = \frac{\Omega_w - \Omega_r}{V_T}, \tag{6}$$

where V_T is the nominal traveling speed of the wheel-set; V_{wx} and V_{wz} are the velocities of the wheel at contact point in the longitudinal and lateral direction, respectively; V_{rx} and V_{rz} are the velocities of the rail at contact point in the

longitudinal and lateral direction, respectively; Ω_w and Ω_r are the rotational velocities of spin motions of the wheel and rail at contact point, respectively. For large creepage ratios, Kalker's linear creepage theory may cause some errors in calculating creeping forces. Johnson's nonlinear creepage law (Kalker, 1990) can be used to modify Kalker's linear creepage theory.

The vehicle subsystem and the track subsystem are coupled through contacts between the wheels and rails. As shown in Fig. 2, the contact forces transmitted from the wheels to the left and right rails in the Y and Z directions can be expressed as

$$F'_{yl} = N_l \cos\delta_l - T_{zl} \sin\delta_l, \quad F'_{zl} = N_l \sin\delta_l + T_{zl} \cos\delta_l, \tag{7a}$$

$$F'_{yr} = N_r \cos\delta_r + T_{zr} \sin\delta_r, \quad F'_{zr} = -N_r \sin\delta_r + T_{zr} \cos\delta_r, \tag{7b}$$

where N and T_z are the normal contact force and the lateral creeping force between the wheel and rail, respectively; δ is the position angle calculated based on the contact angle and the relative rolling angle of the wheel-set; and the subscripts l and r stand for the left and right sides, respectively. The contact forces $F'_{yl}, F'_{yr}, F'_{zl}, F'_{zr}$ at all contact points on the rails constitute the force vector of F_s^c in Eq. (4).

In Eq. (2), F_v^c is the vector of forces exerted by the track subsystem on the vehicle subsystem with respect to the mass center of the wheel-sets. Fig. 2 shows that with the assumption of small displacement, the forces transmitted from the rails to the wheel-set at its mass center can be expressed as

$$F_{vy}^c = F'_{yl} + F'_{yr}, \quad F_{vz}^c = F'_{zl} + F'_{zr}, \tag{8a}$$

$$M_{vx}^c = (F'_{yl} - F'_{yr})B_1/2 - (F'_{zl} + F'_{zr})R_0, \tag{8b}$$

where B_1 is the distance between the left and right contact points; and R_0 is the nominal radius of the wheel. The forces F_{vy}^c, F_{vz}^c, and M_{vx}^c acting on all the wheel-sets of the vehicle constitute the force vector F_v^c in Eq. (2).

2.4. Rail irregularity

Rail irregularities provide important self-excitation in a coupled vehicle–rack system. Rail irregularities are, however, of random nature, and their statistical characteristics are influenced by many factors. For engineering applications, rail irregularities can be approximately regarded as stationary stochastic processes which can be simulated by numerical methods. The wheel hunting is usually omitted in the vehicle–track analysis due to its weak effect.

In this study, the lateral, vertical, and rotational irregularities are all assumed to be zero-mean stationary Gaussian random processes. The rail irregularity profile $r(x)$ can then be generated using a simple inverse Fourier transform:

$$r(x) = \sum_{k=1}^{N} \sqrt{2S(f_k)\Delta f} \cos(2\pi f_k x + \theta_k), \tag{9a}$$

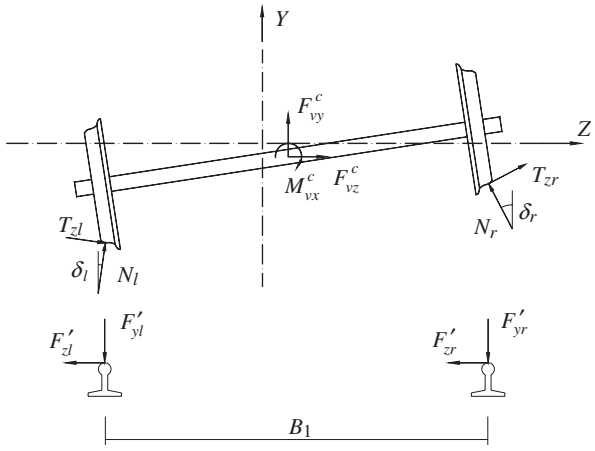

Fig. 2. Contact forces on wheel-set and rails.

$$f_k = (k-1)\Delta f + \frac{\Delta f}{2}, \quad k = 1, 2, \ldots, N, \tag{9b}$$

where $S(f_k)$ is the PSD function (m^3/cycle) of the rail irregularity; f_k is the spatial frequency (cycle/m); Δf is the increment of spatial frequency; and θ_k is the random phase angle uniformly distributed from 0 to 2π.

3. Wind forces on ground vehicles

Wind forces acting on a ground vehicle in cross-wind can be divided into two parts: the steady and unsteady aerodynamic forces. The steady wind forces are due to the mean wind speed component and the unsteady wind forces are caused by the fluctuating wind speed components of natural wind.

The mean wind speed is assumed to be horizontal and normal to the direction of motion of the vehicle in this study. Only wind forces acting on the car body of the vehicle are taken into account. Wind forces acting on the car body of the vehicle refer mainly to drag, lift and moment as shown in Fig. 3. If the vehicle considered is not the first or last vehicle in a long train, the conventional strip theory and quasi-static theory for long-span bridge decks can be applied to the aerodynamics of the vehicle (Scanlan and Gade, 1977; Lin and Yang, 1983).

As shown in Fig. 3, the instantaneous wind velocity V and its angle of incidence α can be given by

$$V^2 = (\bar{u}+u)^2 + w^2, \quad \alpha = \arctan\left(\frac{w}{\bar{u}+u}\right), \tag{10}$$

where $\bar{u}$ is the mean wind speed component; u and w are the longitudinal and vertical fluctuating wind speed components, respectively.

Since the vehicle runs along the track at a constant velocity V_T, the wind velocity V_R relative to the vehicle and its yaw angle φ can be derived as

$$V_R^2 = V_T^2 + V^2 = V_T^2 + (\bar{u}+u)^2 + w^2, \tag{11a}$$

$$\tan\varphi = \sqrt{(\bar{u}+u)^2 + w^2}/V_T. \tag{11b}$$

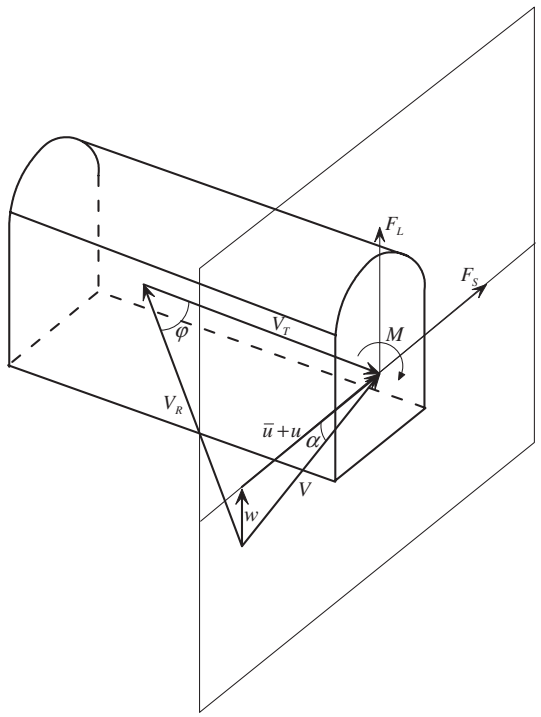

Fig. 3. Wind forces on a moving vehicle.

In most locations, the horizontal fluctuation u and the vertical fluctuation w are considerably smaller than the mean wind speed $\bar{u}$. The higher order fluctuations in Eqs. (10) and (11), such as u^2, w^2, uw, can be neglected, which leads to

$$V^2 = \bar{u}^2 + 2\bar{u}u, \quad \alpha \approx \arctan\left(\frac{w}{\bar{u}}\right), \tag{12}$$

$$V_R^2 = V_T^2 + \bar{u}^2 + 2\bar{u}u, \quad \varphi \approx \arctan\left(\frac{\bar{u}}{V_T}\right). \tag{13}$$

Based on quasi-steady theory, the aerodynamic forces on a moving railway vehicle can be expressed as follows:

$$F_S = \tfrac{1}{2}\rho A V_R^2 C_{F_S}(\alpha, \varphi), \tag{14a}$$

$$F_L = \tfrac{1}{2}\rho A V_R^2 C_{F_L}(\alpha, \varphi), \tag{14b}$$

$$M = \tfrac{1}{2}\rho A H V_R^2 C_M(\alpha, \varphi), \tag{14c}$$

where F_S, F_L and M are the side force, vertical force and rolling moment with respect to the mass center of the car body in the car body coordinate system, respectively, ρ is the air density, A is the reference area, H is the reference height, which is taken as the height of the car body, C_{F_S}, C_{F_L} and C_M are the aerodynamic force coefficients, which are the function of incidence angle α and yaw angle φ. Aerodynamic pitch and yawing moments on a long train are small and neglected in this study. The aerodynamic coefficients can be expanded in Taylor's series form at $\alpha = 0$ as

$$C_i(\alpha, \varphi) = C_i(\varphi) + C_i'(\varphi)\alpha \approx C_i(\varphi) + C_i'(\varphi)\frac{w}{\bar{u}}, \tag{15}$$

where $C_i(\varphi)$ and $C_i'(\varphi)$ $(i = F_S, F_L, M)$ are the side force, lift force and moment coefficients and their derivatives at $\alpha = 0$.

By substituting Eqs. (12), (13) and (15) into Eq. (14) and after some manipulations, wind forces on the car body can be obtained:

$$F_S = \frac{1}{2}\rho A \bar{V}_R^2 C_{F_S}(\varphi) + \frac{1}{2}\rho A \bar{V}_R^2 \left[C_{F_S}(\varphi)\frac{2\bar{u}u}{\bar{V}_R^2} + C'_{F_S}(\varphi)\frac{w}{\bar{u}} \right], \tag{16a}$$

$$F_L = \frac{1}{2}\rho A \bar{V}_R^2 C_{F_L}(\varphi) + \frac{1}{2}\rho A \bar{V}_R^2 \left[C_{F_L}(\varphi)\frac{2\bar{u}u}{\bar{V}_R^2} + C'_{F_L}(\varphi)\frac{w}{\bar{u}} \right], \tag{16b}$$

$$M = \frac{1}{2}\rho A H \bar{V}_R^2 C_M(\varphi) + \frac{1}{2}\rho A H \bar{V}_R^2 \left[C_M(\varphi)\frac{2\bar{u}u}{\bar{V}_R^2} + C'_M(\varphi)\frac{w}{\bar{u}} \right], \tag{16c}$$

where $\bar{V}_R^2 = V_T^2 + \bar{u}^2$. In the above equations, the first term in each case is the steady aerodynamic force and the last two terms are called the unsteady aerodynamic or buffeting forces. The aerodynamic admittance functions are often invoked to reduce the errors involved in quasi-steady theory for the unsteady aerodynamic forces as follows:

$$F_S^{bu} = \frac{1}{2}\rho A \bar{V}_R^2 \left[\chi_{F_S u}(n) C_{F_S}(\varphi)\frac{2\bar{u}u}{\bar{V}_R^2} + \chi_{F_S w}(n) C'_{F_S}(\varphi)\frac{w}{\bar{u}} \right], \tag{17a}$$

$$F_L^{bu} = \frac{1}{2}\rho A \bar{V}_R^2 \left[\chi_{F_L u}(n) C_{F_S}(\varphi)\frac{2\bar{u}u}{\bar{V}_R^2} + \chi_{F_L w}(n) C'_{F_S}(\varphi)\frac{w}{\bar{u}} \right], \tag{17b}$$

$$M^{bu} = \frac{1}{2}\rho A H \bar{V}_R^2 \left[\chi_{Mu}(n) C_M(\varphi)\frac{2\bar{u}u}{\bar{V}_R^2} + \chi_{Mw}(n) C'_M(\varphi)\frac{w}{\bar{u}} \right], \tag{17c}$$

where $\chi_{F_S u}(n)$, $\chi_{F_L u}(n)$, $\chi_{F_S w}(n)$, $\chi_{F_L w}(n)$, $\chi_{Mu}(n)$, and $\chi_{Mw}(n)$ are the aerodynamic transfer functions between the fluctuating wind velocities and aerodynamic forces, and n is the frequency in Hz. The absolute magnitudes of these transfer functions are called the aerodynamic admittance functions.

Obviously, the fluctuation components of turbulence, u and w, should be given to determine the unsteady aerodynamic forces. In this study, the turbulent wind speeds, u and w, are simulated at a series of points along a horizontal line passing through the mass center of the vehicle. The two-side cross-spectral density matrix $\mathbf{S}^{\mathbf{0}}(\omega)$ of each

fluctuation component is given by

$$\mathbf{S}^0(\omega)=\begin{bmatrix} S^0_{11}(\omega) & S^0_{12}(\omega) & \cdots & S^0_{1n}(\omega) \\ S^0_{21}(\omega) & S^0_{22}(\omega) & \cdots & S^0_{2n}(\omega) \\ \vdots & \vdots & \ddots & \vdots \\ S^0_{n1}(\omega) & S^0_{n2}(\omega) & \cdots & S^0_{nn}(\omega) \end{bmatrix}, \tag{18}$$

where n is the number of points where the fluctuation component is simulated. The simulation is performed using the following formula:

$$v_j(t)=2\sqrt{\Delta\omega}\sum_{m=1}^{j}\sum_{l=1}^{N}|H_{jm}(\omega_l)|\cos(\omega_l t-\theta_{jm}(\omega_l)+\phi_{ml}), \tag{19a}$$

$$\omega_l=(l-1)\Delta\omega+\Delta\omega/2,\quad l=1,2,\ldots,N, \tag{19b}$$

where v stands for either u or w; N is a sufficiently large number; $\Delta\omega=\omega_{\mathrm{up}}/N$ is the frequency increment; ω_{up} is the upper cut-off frequency with the condition that, when $\omega>\omega_{\mathrm{up}}$, the value of $\mathbf{S}^0(\omega)$ is trivial; ϕ_{ml} is the sequence of independent random phase angles uniformly distributed over the interval $[0, 2\pi]$; $H_{jm}(\omega)$ is a typical element of matrix $\mathbf{H}(\omega)$, which is defined by the Cholesky decomposition of cross-spectral density matrix $\mathbf{S}^0(\omega)$; and $\theta_{jm}(\omega)$ is the complex angle of $H_{jm}(\omega)$.

The time histories of the unsteady aerodynamic forces at n points are computed using Eq. (17) in which fluctuating wind speeds are interpolated based on Taylor's frozen turbulence hypothesis in predicting dynamic response of the coupled vehicle–track system in cross-wind. Furthermore, when the aerodynamic admittance should be taken into consideration, equivalent wind spectra including the admittance functions can be used to simulate the equivalent fluctuating wind speeds.

4. Numerical solution

The dynamic response of coupled vehicle–track system in cross-wind is predicted in the time domain in this study. Since the coupled system is a nonlinear system due to nonlinear contacts between wheels and rails, the Hilber–Hughes–Taylor α-method (Hughes, 1987), which is regarded as a modified Newmark method, is used to find numerical solution to avoid spurious high-frequency oscillations in nonlinear contact problems.

In the traditional Newmark method (Chaudhary and Bathe, 1986), the velocity $\dot{X}_{t+\Delta t}$ and displacement $X_{t+\Delta t}$ at time $t+\Delta t$ are calculated in terms of the acceleration $\ddot{X}_{t+\Delta t}$ at time $t+\Delta t$ using the following algorithm:

$$\dot{X}_{t+\Delta t}=\dot{X}_t+(1-\gamma)\ddot{X}_t\Delta t+\gamma\ddot{X}_{t+\Delta t}\Delta t, \tag{20a}$$

$$X_{t+\Delta t}=X_t+\dot{X}_t\Delta t+[(\tfrac{1}{2}-\beta)\ddot{X}_t+\beta\ddot{X}_{t+\Delta t}]\Delta t^2, \tag{20b}$$

where γ and β are the two weighting parameters. Let us denote

$$c_0=\frac{1}{\beta\Delta t^2},\quad c_1=\frac{\gamma}{\beta\Delta t},\quad c_2=\frac{1}{\beta\Delta t},\quad c_3=\frac{1}{2\beta}-1, \tag{21a}$$

$$c_4=\frac{\gamma}{\beta}-1,\quad c_5=\frac{\Delta t}{2}\left(\frac{\gamma}{\beta}-2\right),\quad c_6=\Delta t(1-\gamma),\quad c_7=\Delta t\gamma. \tag{21b}$$

Eq. (20) can be rewritten as

$$\ddot{X}_{t+\Delta t}=c_0(X_{t+\Delta t}-X_t)-c_2\dot{X}_t\Delta t-c_3\ddot{X}_t, \tag{22a}$$

$$\dot{X}_{t+\Delta t}=\dot{X}_t+c_6\ddot{X}_t+c_7\ddot{X}_{t+\Delta t}. \tag{22b}$$

To use the α-method, the equation of motion of either the vehicle subsystem or the track subsystem is modified as

$$M\ddot{X}_{t+\Delta t}+(1+\alpha)C\dot{X}_{t+\Delta t}-\alpha C\dot{X}_t+(1+\alpha)KX_{t+\Delta t}-\alpha KX_t=(1+\alpha)F_{t+\Delta t}-\alpha F_t, \tag{23}$$

where $-1/3 \leqslant \alpha \leqslant 0$. Inserting Eq. (22) into Eq. (23) then yields

$$\hat{K} X_{t+\Delta t} = \hat{F}_{t+\Delta t}, \tag{24}$$

where

$$\hat{K} = c_0 M + (1+\alpha)K + c_1(1+\alpha)C,$$

$$\hat{F}_{t+\Delta t} = (1+\alpha)F_{t+\Delta t} + M(c_0 X_t + c_2 \dot{X}_t + c_3 \ddot{X}_t) + (1+\alpha)C(c_1 X_t + c_4 \dot{X}_t + c_5 \ddot{X}_t) - \alpha(F_t - C\dot{X}_t - KX_t).$$

By using Eq. (24), the displacement of either subsystem can be solved at time step $t + \Delta t$, and the corresponding velocity and acceleration of the subsystem can then be obtained using Eq. (22). Clearly, if $\alpha = 0$, the α-method is reduced to the traditional Newmark method. It is shown that when the parameters are selected as

$$\gamma = (1-2\alpha)/2, \quad \beta = (1-\alpha)^2/4, \tag{25}$$

the α-method results in unconditional stability and second-order accuracy and improves convergence in nonlinear contact problems.

The main procedure for the numerical integration of the equations of motion of the coupled vehicle and track system in cross-wind can be summarized as follows:

(a) estimate the motion of wheel-sets based on the motion of two rails and rail irregularities;

(b) estimate the contact forces on the wheel-set based on the contact theory through iteration;

(c) compute wind forces and solve Eq. (2) to find the first approximation of motion of vehicle subsystem;

(d) because of the nonlinear nature of contact forces, an internal iteration is required until the solution of Eq. (2) converges;

(e) the contact forces computed from the vehicle subsystem are then applied to the track subsystem, and Eq. (4) is integrated to find the new approximation of motion of the track subsystem;

(f) the steps (a)–(e) are repeated, until the convergence is reached for both Eq. (2) and Eq. (4). At this point a new time step can be started from (a).

5. Case study

A computer program is written based on the framework discussed above and is used to perform a case study, in which dynamic responses of a railway vehicle running on a straight track subsystem in cross-wind are predicted, and the safety and comfort performance of the moving vehicle in cross-wind are assessed.

5.1. Vehicle and track models

The railway vehicle model consists of seven rigid bodies: one car body, two bogies, and four wheel-sets. The seven rigid bodies are connected with springs and dashpots, forming a vehicle subsystem of 27 degrees of freedom. The main parameters of the railway vehicle used in the case study are listed in Table 1. The height and length of the car body are 3.2 and 22.5 m, respectively. The average static axle load of the vehicle is 10 150 kg. The fundamental frequency of the railway vehicle is 0.49 Hz in the lateral direction and 1.06 Hz in the vertical direction.

The railway track model includes two rails and a series of sleepers and ballasts, which are connected to each other using springs and dashpots. The main parameters of the railway track subsystem are listed in Table 2. The total length of the track subsystem considered in this case study is 1090 m. The spacing distance between two adjacent sleepers is 0.545 m. Thus, there are a total of 2001 sleepers. The distance between the centers of two rails is 1.435 m. Both the vehicle and track subsystems used in this study represent a conventional railway line in China (Zhai, 2002).

The cross-section profiles of both rails and wheels are important in considering vehicle and track interaction. The TB60 rail and worn wheel, commonly used in China for analysis of vehicle and track interaction, are adopted in this study. Then, the relationships of the relative rolling angle, the contact angle, and others with the lateral displacement of wheel-set are found (Zhai, 2002). Fig. 4 shows the relative rolling angle and the contact angle as the function of the lateral displacement of the wheel-set at a zero yaw angle. The sign of the angles complies with the X–Y–Z coordinate system shown in Fig. 1. Clearly, there relations are strongly nonlinear.

5.2. Wind forces on vehicle

For simulation of the railway vehicle and track interaction in cross-wind, the aerodynamic data, including both steady force coefficients and turbulence characteristics, for the moving vehicle are required. Several researchers have acquired some valuable results in this aspect using either an experimental or a numerical approach.

Table 1
Main parameters of the vehicle model used in the case study

Parameter	Units	Value
Half distance of two wheel-sets (q)	m	1.200
Half distance of bogie (s)	m	9.0
Half span of the 1st suspension system (a)	m	0.978
Half span of the 2nd suspension system (b)	m	0.978
Mass of wheel-set (M_w)	kg	1900
Mass moment of inertia of wheel-set around x-axis (I_w)	kg m^2	1067
Distance between car body and 2nd suspension system (h_1)	m	1.415
Distance between 2nd suspension system and bogie (h_2)	m	−0.081
Distance between bogie and wheel-set (h_3)	m	0.14
Radius of wheel (R_w)	m	0.4575
Mass of bogie (M_b)	kg	1700
Mass moment of inertia of bogie around x-axis (I_{bX})	kg m^2	1600
Mass moment of inertia of bogie around y-axis (I_{bY})	kg m^2	1700
Mass moment of inertia of bogie around z-axis (I_{bZ})	kg m^2	1700
Mass of car body (M_c)	kg	29 600
Mass moment of inertia of car body around x-axis (I_{cX})	kg m^2	58 020
Mass moment of inertia of car body around y-axis (I_{cY})	kg m^2	2 139 000
Mass moment of inertia of car body around z-axis (I_{cZ})	kg m^2	2 139 000
Lateral damping of 1st suspension system (per side) (C_{h1})	N s/m	25 000
Lateral damping of 2nd suspension system (per side) (C_{h2})	N s/m	0
Lateral stiffness of 1st suspension system (per side) (K_{h1})	N/m	5 100 000
Lateral stiffness of 2nd suspension system (per side) (K_{h2})	N/m	300 000
Vertical damping of 1st suspension system (per side) (C_{v1})	N s/m	30 000
Vertical damping of 2nd suspension system (per side) (C_{v2})	N s/m	108 700
Vertical stiffness of 1st suspension system (per side) (K_{v1})	N/m	873 000
Vertical stiffness of 2nd suspension system (per side) (K_{v2})	N/m	410 000

Table 2
Main parameters of the track model used in the case study

Parameter	Unit	Value
Distance between the centers of two rails	m	1.435
Sleeper spacing	m	0.545
Mass of steel rail per unit length	kg/m	60.64
Mass of sleeper	kg	237
Lumped mass of ballast	kg	739
Vertical bending stiffness of rail	MN m^2	6.62
Lateral bending stiffness of rail	MN m^2	1.079
Thickness of ballasts	m	0.45
Density of ballasts	kg/m^3	1800
Elastic modulus of ballasts	MPa/m	1.1×10^8
Vertical stiffness of pads and fasteners	MN/m	120
Vertical damping of pads and fasteners	kN s/m	75
Elastic modulus of roadbeds	MPa/m	8.0×10^7
Vertical stiffness of roadbeds	MN/m	65
Vertical damping of roadbeds	kN s/m	31

The steady coefficients of the side force, vertical force and rolling moment on the vehicle used in this case study are depicted in Fig. 5 as a function of the wind yaw angle. These coefficients are quite similar to those reported by Baker et al. (2003). Also given in Fig. 5 is the derivative of steady side-force coefficient with respect to wind inclination at zero

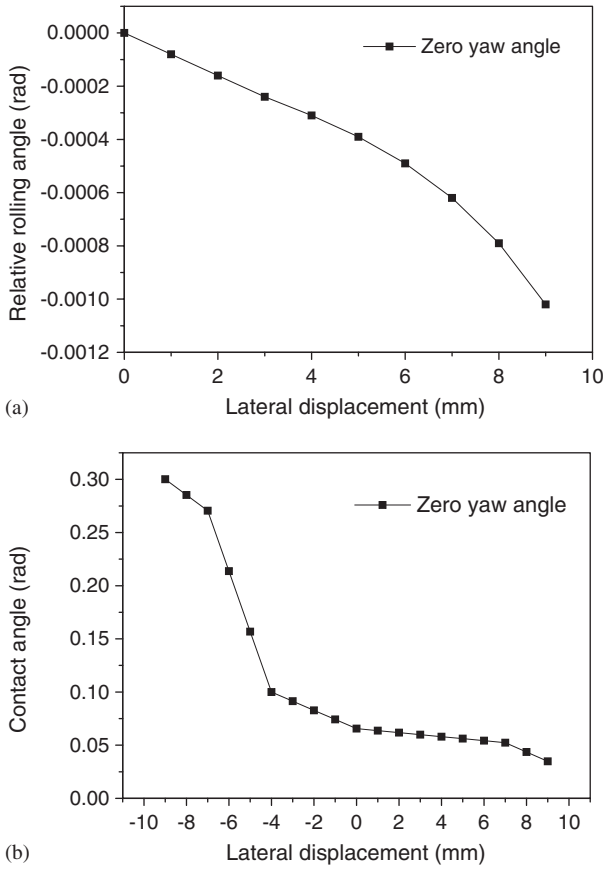

Fig. 4. Relationship of relative rolling angle and contact angle with lateral displacement of wheel-set: (a) relative rolling angle; (b) contact angle.

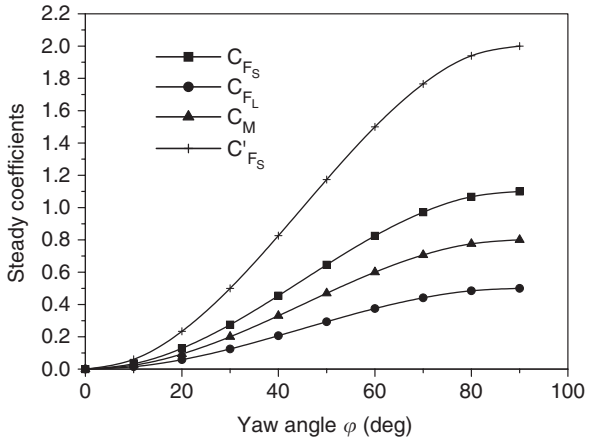

Fig. 5. Steady aerodynamic coefficients for the vehicle used in the case study.

angle. The derivatives of other force (moment) coefficients are not available. It is noted that the steady coefficients of side force, vertical force, and rolling moment at the yaw angle of 90° are 1.1, 0.5, and 0.8, respectively.

In the simulation of unsteady aerodynamic forces on the vehicle, the following von Kármán longitudinal and vertical wind auto-spectra are adopted (Simiu and Scanlan, 1996):

$$\frac{nS_{uu}(n)}{\sigma_u^2} = \frac{4\dfrac{L_u n}{\bar{u}}}{\left[1 + 70.8\left(\dfrac{L_u n}{\bar{u}}\right)^2\right]^{5/6}}, \tag{26a}$$

$$\frac{nS_{ww}(n)}{\sigma_w^2} = \frac{4\dfrac{L_w n}{\bar{u}}\left[1 + 755\left(\dfrac{L_w n}{\bar{u}}\right)^2\right]}{\left[1 + 283\left(\dfrac{L_w n}{\bar{u}}\right)^2\right]^{11/6}}, \tag{26b}$$

where σ_u and σ_w are the standard deviations of fluctuating wind in the longitudinal and vertical direction, which are taken as $0.15\bar{u}$ and $0.075\bar{u}$, respectively, in this study, n is the frequency in Hz, and L_u and L_w are the integral length scales of fluctuating wind in the longitudinal and lateral directions, which are set to 45 and 15 m, respectively, in this study.

The turbulence coherence which defines the statistical dependency between the turbulence components at two different points is given by

$$\sqrt{\text{coh}} = \exp\left(-\frac{CDn}{\bar{u}}\right), \tag{27}$$

where C is the decay factor selected as 10 for longitudinal turbulence and 8 for vertical turbulence; D is the distance between the two points. Because of lack of information, the aerodynamic admittance functions for the unsteady aerodynamic forces are assumed to be equal to unity, and the co-spectra between the longitudinal and vertical turbulence components are set to zero.

Based on the wind spectra and coherence functions, time histories of longitudinal and vertical fluctuating wind speeds are simulated along the line of track subsystem at the level of vehicle mass center and at a distance interval of 5 m. The total number of the time histories is 219 in either the longitudinal direction or the vertical direction. The duration of each time history is 164 s, and the sampling frequency is 50 Hz. The unsteady aerodynamic forces on the moving vehicle can then be computed using Eq. (17) and applied to the vehicle based on Taylor's frozen turbulence hypothesis with a proper interpolation at a given time.

5.3. Rail irregularity

In this case study, vertical and lateral irregularities are considered for both the right and left rails of the track subsystem. The rail irregularity in railway engineering is often represented by a one-sided PSD function. The PSD functions of rail irregularities developed by the Research Institute of China Railway Administration (Zhai, 2002) are used in this case study. All of rail irregularities are expressed using a unified rational formula as

$$S(f) = \frac{A(f^2 + Bf + C)}{f^4 + Df^3 + Ef^2 + Ff + G}\ \text{mm}^2/\text{m}^{-1}, \tag{28}$$

where $f = 1/\lambda$ is the spatial frequency in cycle/m (λ is the wavelength); A to G are the specific parameters but they are different for vertical and lateral rail irregularities. The values of these parameters can be found in Zhai (2002). Fig. 6 displays simulated vertical and lateral rail irregularities of the right and left rails. In the simulation, the length of the track subsystem is taken as 1090 m and the sampling points are 2001, which is the same as the number of sleepers.

5.4. Response of coupled vehicle–track system in cross-wind

Let us consider that the vehicle runs at a constant velocity of 160 km/h in cross-wind. The wind is normal to the motion of the vehicle and of 20 m/s at the level of the vehicle mass center. The relative wind velocity V_R is, therefore, 48.7 m/s and the wind yaw angle φ is 24°.

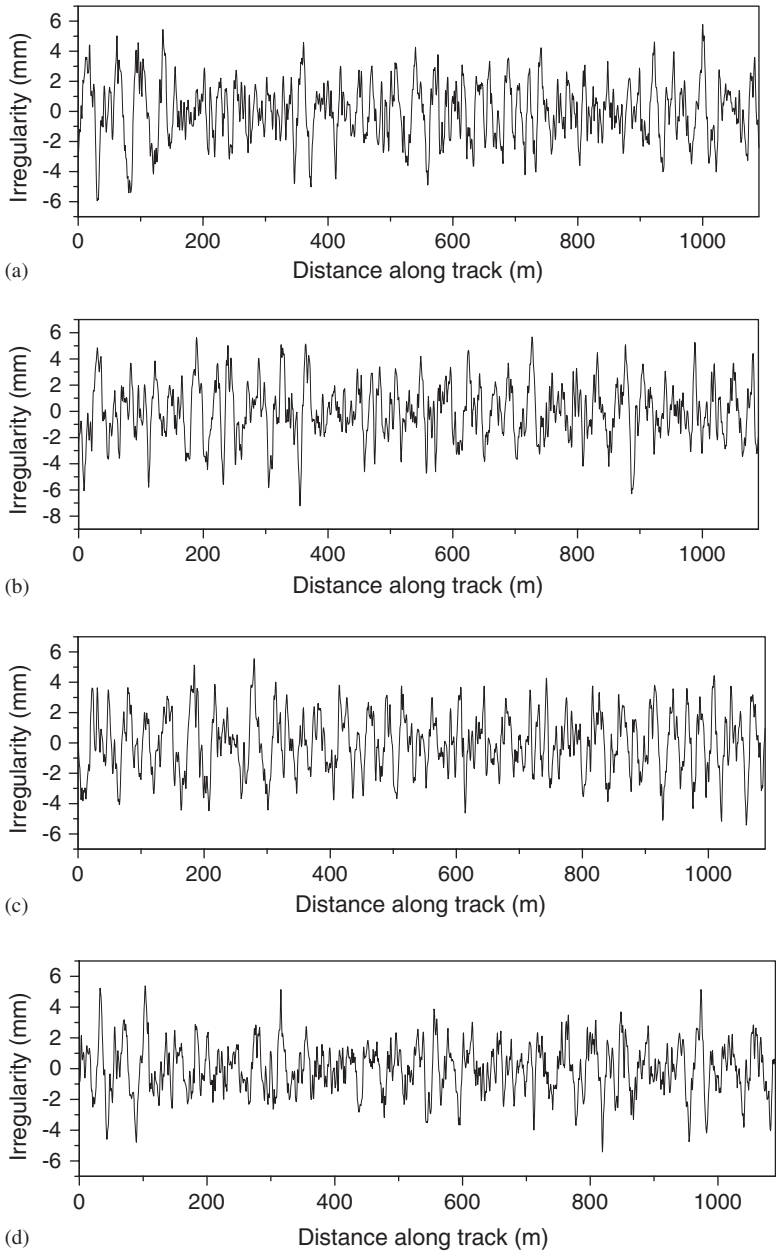

Fig. 6. Vertical and lateral rail irregularities: (a) vertical irregularity of left rail; (b) vertical irregularity of right rail; (c) lateral irregularity of left rail; (d) lateral irregularity of right rail

Fig. 7 depicts the time histories of vertical and lateral displacement responses of the car body at its center with and without wind forces. Fig. 8 displays the time history of lateral displacement response of the first wheel-set of the vehicle with and without wind forces. It can be seen that both steady and unsteady aerodynamic forces have significant influence on the vertical and lateral displacement responses of the moving vehicle, in particular in the lateral direction where the lateral displacement of the car body is very small without wind forces but increases significantly under wind forces. Figs. 9 and 10 show the time histories of vertical and lateral acceleration responses of the car body at its center without and with wind forces, respectively. Compared with the displacement responses of the car body, effects of unsteady aerodynamic forces on acceleration responses of the car body are relatively smaller. Figs. 11 and 12 show the horizontal and vertical contact forces between the first wheel-set and rails on both windward and leeward sides without

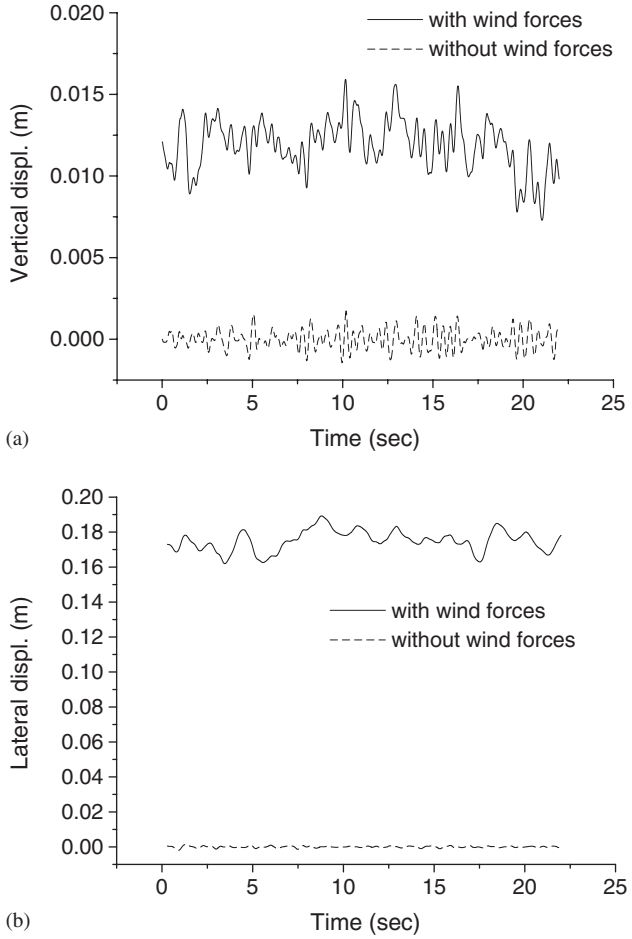

Fig. 7. Displacement responses of the car body at its center ($\bar{u} = 20\,\mathrm{m/s}$, $V_T = 160\,\mathrm{km/h}$): (a) vertical displacement; (b) lateral displacement.

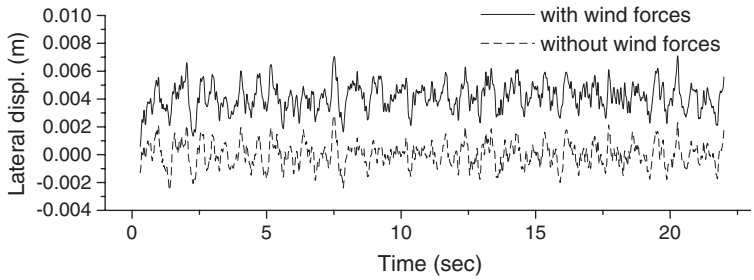

Fig. 8. Lateral displacement responses of the first wheel-set ($\bar{u} = 20\,\mathrm{m/s}$, $V_T = 160\,\mathrm{km/h}$).

and with wind forces, respectively. It can be seen that, without wind forces, the horizontal contact forces on the windward rail and the leeward rail are similar in magnitude but opposite in direction. The vertical contact forces on the windward rail and the leeward rail are similar in both magnitude and direction. With wind forces, both the horizontal and vertical contact forces on the leeward side are much larger than those on the windward side. The horizontal and vertical contact forces on the leeward side are also much larger with wind forces than without wind forces. Wind forces thus certainly affect the safety and comfort performance of the moving railway vehicle.

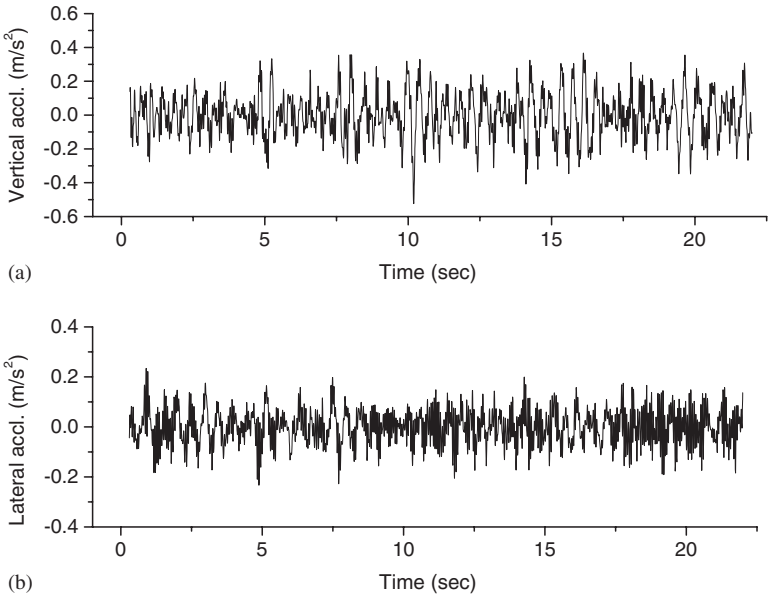

Fig. 9. Acceleration responses of the car body at its center without wind forces ($V_T = 160$ km/h); (a) vertical acceleration; (b) lateral acceleration.

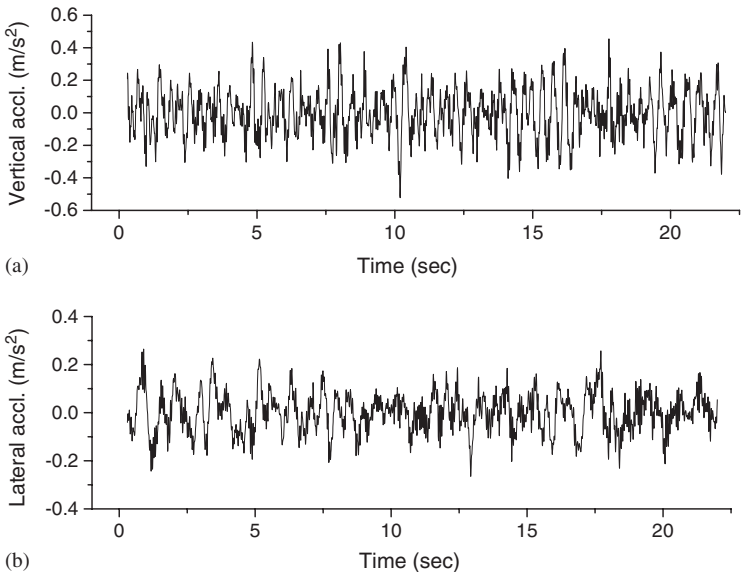

Fig. 10. Acceleration responses of the car body at its center with wind forces ($\bar{u} = 20$ m/s, $V_T = 160$ km/h): (a) vertical acceleration; (b) lateral acceleration.

To know if the elasticity of the track subsystem will affect the coupled vehicle–track system in cross-wind, the responses of the coupled vehicle–track system in cross-wind are also computed using a rigid track subsystem, in which the stiffness of all springs in the original track subsystem are assumed to be infinite large. The displacement responses of the car body running on the elastic and rigid track subsystem are plotted in Fig. 13 for both vertical and lateral directions. It can be observed that both the lateral and vertical displacement responses of the car body running on the elastic track subsystem are almost the same as those running on the rigid track subsystem. This is because the stiffness of the track subsystem used in this study is much higher than that of the railway vehicle. However, if the stiffness of the

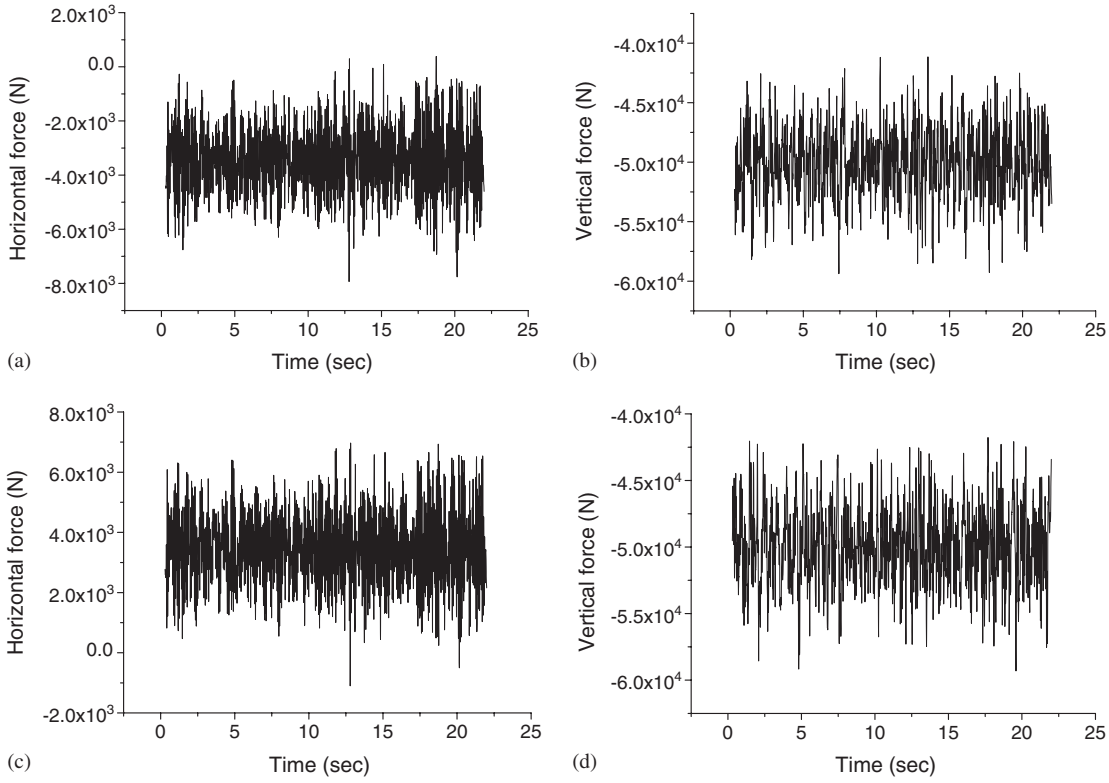

Fig. 11. Horizontal and vertical contact forces between the first wheel-set and rails without wind forces ($V_T = 160$ km/h): (a) windward side; (b) windward side; (c) leeward side; (d) leeward side.

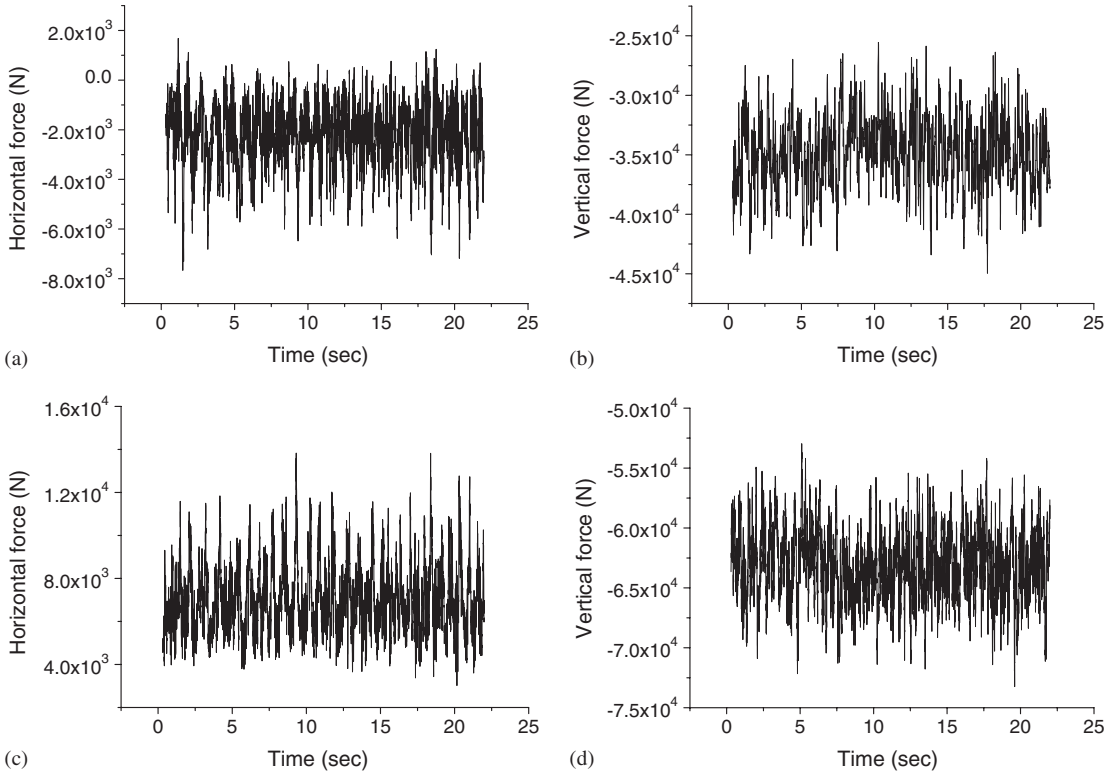

Fig. 12. Horizontal and vertical contact forces between the first wheel-set and rails with wind forces ($\bar{u} = 20$ m/s, $V_T = 160$ km/h): (a) windward side; (b) windward side; (c) leeward side; (d) leeward side.

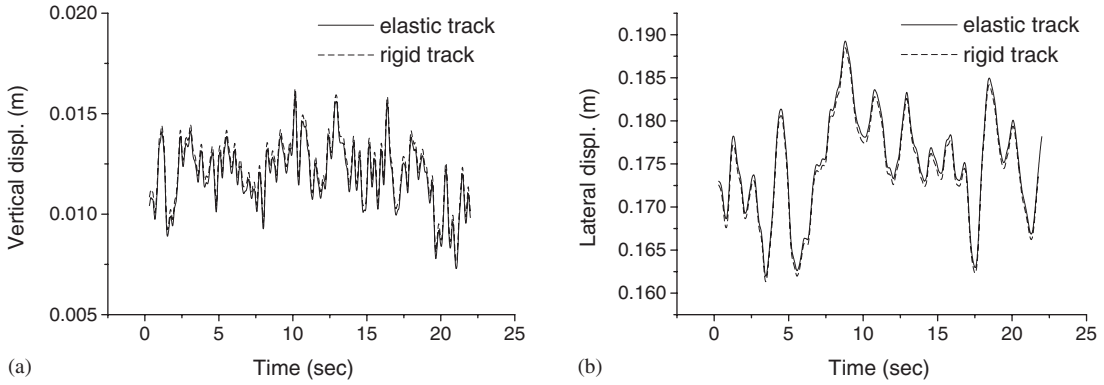

Fig. 13. Comparison of displacement responses of car body running on the elastic and rigid track subsystem ($\bar{u} = 20\,\mathrm{m/s}$, $V_T = 160\,\mathrm{km/h}$): (a) vertical displacement; (b) lateral displacement.

track subsystem is comparable with that of the vehicle, the elastic track subsystem rather than the rigid track subsystem should be used.

5.5. Safety and ride comfort performance

The safety of a railway vehicle concerns mainly derailment. There are two important factors that should be considered in the evaluation of the safety of a railway vehicle. One is the derail factor defined as the ratio of lateral force Q acting on the wheel to the total vertical force P acting on the same wheel. The total vertical force is the sum of the self-weight of the vehicle per wheel and the dynamic vertical forces on the wheel. The other factor is the load reduction factor defined as the ratio of the reduction in the vertical force to the static wheel load,

$$\Delta P/P_0 = (P - P_0)/P_0, \tag{29}$$

in which P_0 is the static wheel load and ΔP is the reduction in the wheel load with respect to P_0. The allowable derail factor (Q/P) and load reduction factor specified in the Chinese design guideline are 1.0 and 0.6, respectively (Zhai, 2002). Therefore, if the conditions

$$Q/P \leqslant 1.0, \quad \Delta P/P_0 \leqslant 0.6 \tag{30}$$

are satisfied at the same time, the railway vehicle is said to be safe.

The ride comfort of the passenger coach in a running train can be assessed using the Sperling comfort index that is defined as

$$W = 0.896\left(\frac{a^3}{f}F(f)\right)^{1/10}, \tag{31}$$

where a is the acceleration of the car body in $\mathrm{cm/s^2}$; f is the frequency in Hz; and $F(f)$ is the modification coefficient of frequency. For vertical vibration,

$$F(f) = \begin{cases} 0.325f^2 & (f = 0.5\sim5.9\,\mathrm{Hz}), \\ 400/f^2 & (f = 5.9\sim20\,\mathrm{Hz}), \\ 1 & (f > 200\,\mathrm{Hz}); \end{cases} \tag{32a}$$

for lateral vibration,

$$F(f) = \begin{cases} 0.8f^2 & (f = 0.5\sim5.4\,\mathrm{Hz}), \\ 650/f^2 & (f = 5.4\sim26\,\mathrm{Hz}), \\ 1 & (f > 26\,\mathrm{Hz}). \end{cases} \tag{32b}$$

The acceleration response of the car body is random due to random wind forces and rail irregularities and it contains a wide range of vibration frequencies. Thus, the Sperling comfort index is calculated for a series of frequencies based on the Fourier spectrum of the acceleration response time history. Its mean value is then taken for the assessment of the

vehicle comfort. The allowable value of vehicle comfort specified in the Chinese design guideline is 3.0 for both lateral and vertical vibrations.

To investigate the effects of wind speed on the safety and ride comfort of the railway vehicle concerned in this study, both displacement and acceleration responses of the coupled vehicle and track system are computed for mean wind speeds ranging from zero to 30 m/s at 5 m/s intervals. The running speed of the vehicle remains at 160 km/h. The computed results relating to the safety and comfort indexes of the vehicle are listed in Table 3. The variations of the derail factor and the load reduction factor with wind speed are plotted in Fig. 14. It can be seen that the safety of the vehicle is controlled by the load reduction factor rather than the derail factor. Based on the allowable value of the load reduction factor, $\Delta P/P_0 = 0.6$, the critical wind speed should be about 21 m/s. It is also noted that, even at the critical wind speed, the lateral Sperling index is less than 2, indicating that the ride comfort is satisfactory.

Generally speaking, the safety and comfort performance of the vehicle also vary with vehicle speed. However, wind forces on the moving vehicle concerned in this study are dominated by wind speed rather than vehicle speed. It is noted from the analysis that the effects of vehicle speed on the safety and comfort performance are relatively small. Nevertheless, further studies are required to investigate effects of vehicle speed on safety and comfort performance when the required experimental data are available.

6. Concluding remarks

The framework for simulating railway vehicle and track interaction under cross-wind has been presented in this paper. The vehicle subsystem, represented by a 27-degree-of-freedom dynamic system, and the track subsystem,

Table 3
Safety and comfort performance of the vehicle used in the case study

Wind velocity (m/s)	Derailment factor (Q/P)	$\Delta P/P_0$	Lateral Sperling index (W)	$\ddot{Z}_{max}$ (m/s^2)[a]
0.0	0.074	0.285	1.413	0.234
5.0	0.077	0.293	1.413	0.234
10.0	0.087	0.350	1.414	0.236
15.0	0.101	0.446	1.420	0.237
20.0	0.129	0.580	1.537	0.327
25.0	0.156	0.753	1.703	0.437
30.0	0.216	0.969	2.016	0.678

[a] $\ddot{Z}_{max}$ =the maximum lateral acceleration at the center of the car body.

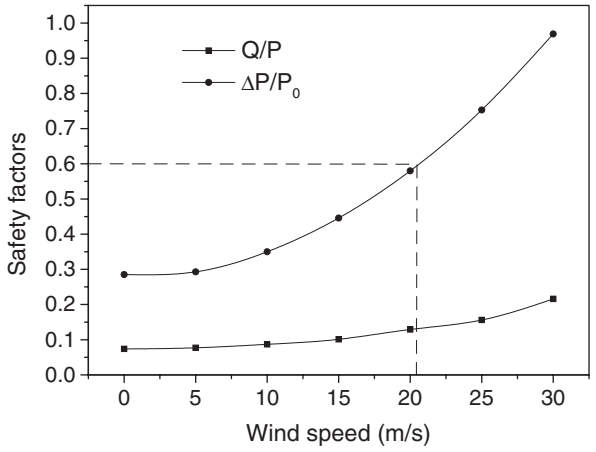

Fig. 14. Variations of safety factors of the moving vehicle with wind speed.

modeled as two continuous beams supported by a discrete-elastic foundation of three layers, are coupled through contacts between wheels and rails, with vertical and lateral rail irregularities included. The steady and unsteady aerodynamic forces on a moving railway vehicle in cross-wind are simulated in the time domain.

The proposed framework is applied to a railway vehicle running on a straight track substructure in cross-wind. The results demonstrate that wind forces have significant effects on vehicle responses, in particular in the lateral direction. The results also show that the lateral and vertical displacement responses of the car body running on the elastic track subsystem are almost the same as those running on the rigid track subsystem for the coupled vehicle–track system considered in this study. Furthermore, the safety of the vehicle is controlled by the load reduction factor rather than the derail factor: the critical wind speed is about 21 m/s when the vehicle speed is 160 km/h (44.4 m/s). The ride comfort performance of the vehicle is satisfactory. It should be noted that all the conclusions made in this paper remain strictly valid only for the particular models and assumptions adopted in this study.

Acknowledgments

The writers are grateful for the financial support from the Research Grants Council of Hong Kong through a RGC research Grant (PolyU5043/01E). The writers would also like to express their sincere thanks to Dr. Y.L. Li of the Southwest Jiaotong University of China for his help in the derivation of wind forces on a moving vehicle.

References

Baker, C.J., 1991a. Ground vehicles in high cross wind, Part I: steady aerodynamic forces. Journal of Fluids and Structures 5, 69–90.

Baker, C.J., 1991b. Ground vehicles in high cross wind, Part II: unsteady aerodynamic forces. Journal of Fluids and Structures 5, 91–111.

Baker, C.J., Jones, J., Lopez-Calleja, F., Numday, J., 2003. Measurements of the cross wind forces on trains. In: Proceedings of 11th International Conference on Wind Engineering. Texas Tech. University, Lubbock, TX, USA, pp. 845–852.

Balzer, Z.A., 1977. Atmospheric turbulence encountered by high-speed ground transport vehicles. Journal of Mechanical Engineering Science 19, 227–235.

Cai, Z., Raymond, G.P., 1992. Theoretical model for dynamic wheel/rail and track interaction. In: Proceedings of 10th International Wheelset Congress. Sydney, Australia, pp. 127–131.

Chaudhary, A.B., Bathe, K.J., 1986. A solution method for static and dynamic analysis of three-dimensional contact problems with friction. Computers and Structures 24, 855–873.

Cooper, R.K., 1984. Atmospheric turbulence with respect to moving ground vehicles. Journal of Wind Engineering and Industrial Aerodynamics 17, 215–238.

Dahlberg, T., 1995. Vertical dynamic train/track interaction verifying a theoretical model by full-scale experiments. Vehicle System Dynamics 24 (Suppl.), 45–57.

Diana, G., Cheli, F., Bruni, S., Collina, A., 1994. Interaction between railroad superstructure and railway vehicles. Vehicle System Dynamics 23 (Suppl.), 75–86.

Grassie, S.L., Gregory, R.W., Harrison, D., Johnson, K.L., 1982. The dynamic response of railway track to high frequency vertical excitation. Journal of Mechanical Engineering Science 24, 77–90.

Hughes, T.J.R., 1987. The Finite Element Method: Linear Static and Dynamic Finite Element Analysis. Prentice-Hall, Inc., Englewood Cliffs, NJ.

Jenkins, H.H., Stephenson, J.E., Clayton, G.A., Morland, G.W., Lyon, D., 1974. The effect of track and vehicle parameters on wheel/rail vertical dynamic forces. Railway Engineering Journal 3 (1), 2–16.

Kalker, J.J., 1990. Three-dimensional Elastic Bodies in Rolling Contact. Kluwer Academic Publishers, Dordrecht.

Knothe, K.L., Grassie, S.L., 1993. Modeling of railway track and vehicle/track interaction at high frequencies. Vehicle System Dynamics 22, 209–262.

Lin, Y.K., Yang, J.N., 1983. Multimode bridge response to wind excitations. ASCE Journal of Engineering Mechanics 109 (2), 586–603.

Newton, S.G., Clark, R.A., 1979. An investigation into the dynamic effects on the track of wheel flats on railway vehicles. Journal of Mechanical Engineering Science 21 (4), 287–297.

Nielsen, J.C.O., 1993. Train/track interaction: coupling of moving and stationary dynamic system. Dissertation, Chalmers University of Technology, Göteborg, Sweden.

Scanlan, R.H., Gade, R.H., 1977. Motion of suspension bridge spans under gusty wind. ASCE Journal of the Structural Division 103 (ST9), 1867–1883.

Simiu, P.D., Scanlan, R.H., 1996. Wind Effects on Structures. Wiley, New York.

Xu, Y.L., Zhang, N., Xia, H., 2004. Vibration of coupled train and cable-stayed bridge systems in cross-wind. Engineering Structures 26, 1389–1406.

Zhai, W., Sun, X., 1994. A detailed model for investigating interaction between railway vehicle and track. Vehicle System Dynamics 23 (Suppl.), 603–614.

Zhai, W.M., 2002. Vehicle–Track Coupling Dynamics, second ed. Chinese Railway Publishing House, Beijing (in Chinese).

Zhai, W.M., Cai, C.B., Guo, S.Z., 1996. Coupling model of vertical and lateral vehicle/track interactions. Vehicle System Dynamics 26 (1), 61–79.